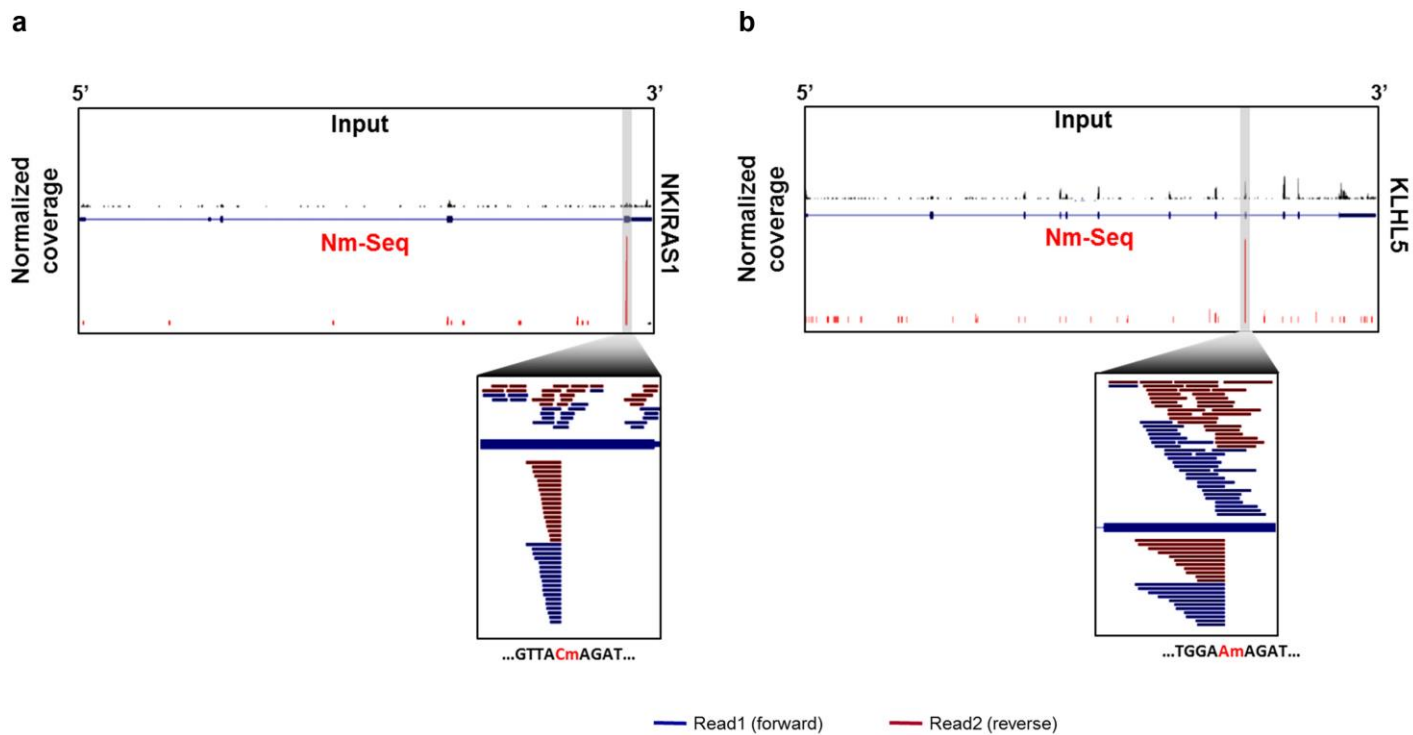


Supplementary Figure 1

Detection of Nm sites in HeLa rRNA

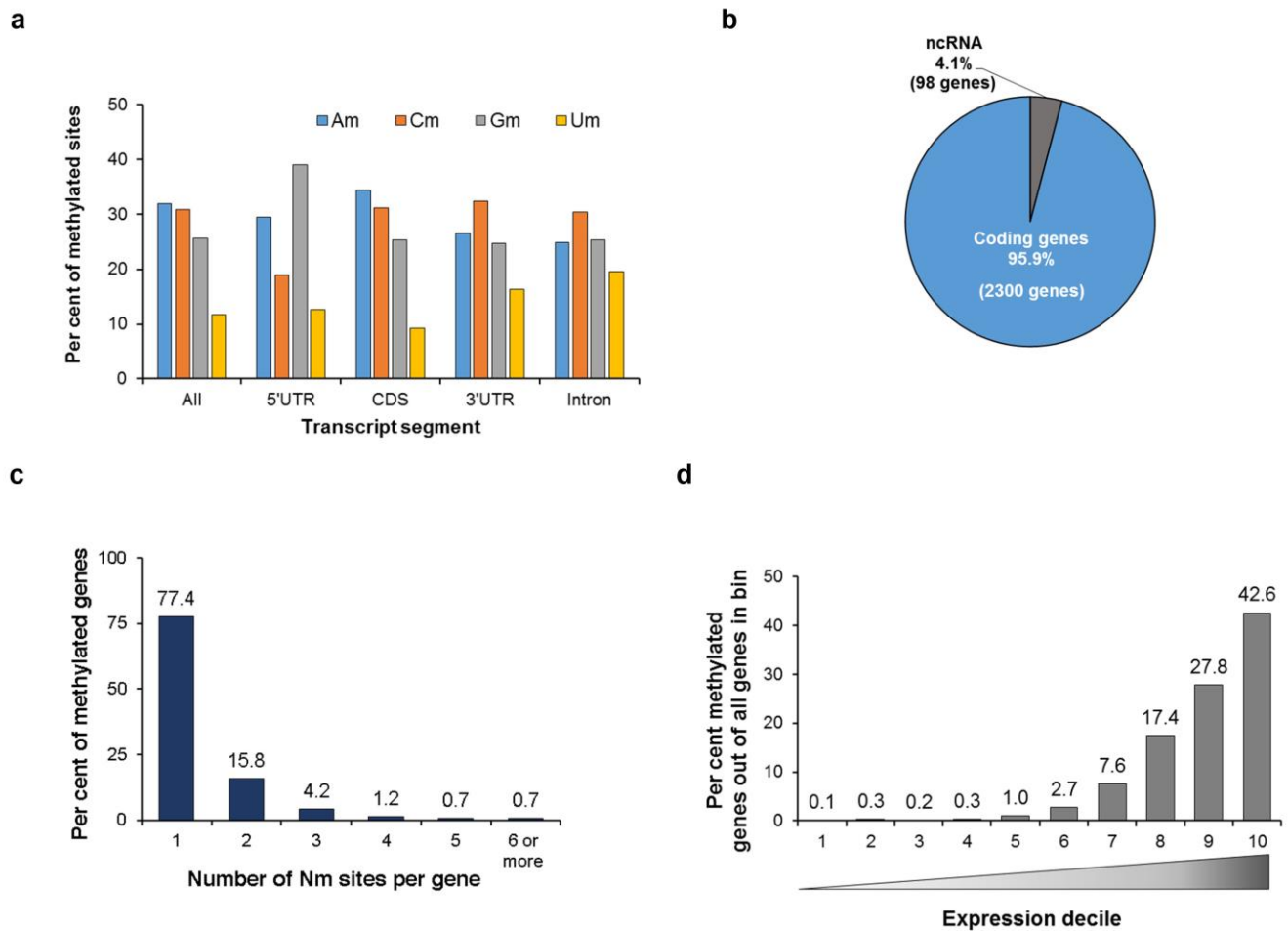
(a-b), Nm-seq profiles of human 18S (a) and 28S (b) rRNA above MCC-determined optimal threshold (blue). Known Nm sites are shown as red bars below. (c-d), Receiver Operating Characteristic (ROC, orange) and Mathews Correlation Coefficient (MCC, green) curves for human 18S (c) and 28S (d) rRNA plotted using increasing normalized 3' end coverage thresholds at each position.



Supplementary Figure 2

Examples of Nm sites in HeLa mRNA.

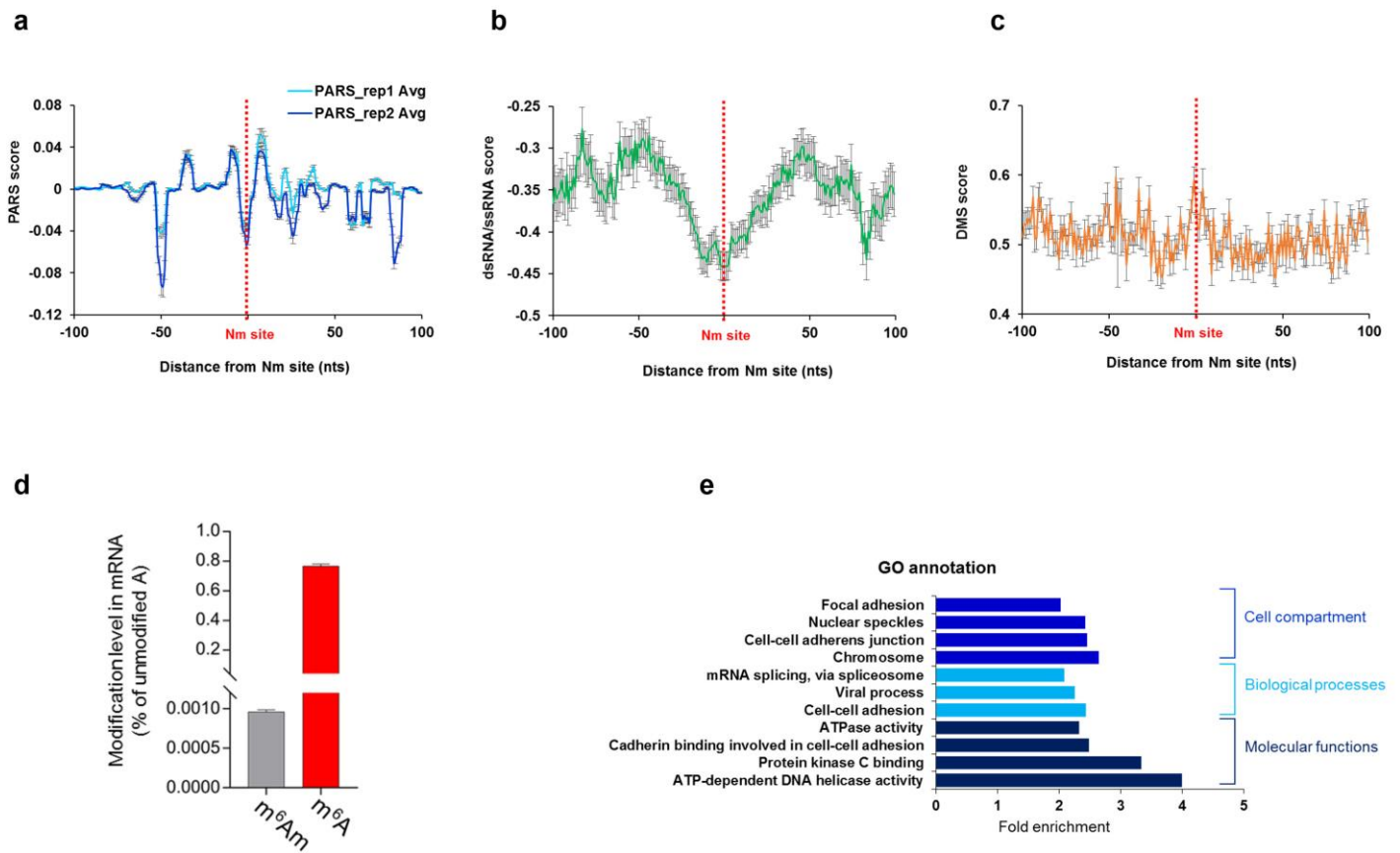
Nm-seq plots of methylated transcripts: **(a)** NKIRAS1 **(b)** KLHL5. Normalized summed sequence coverage of Nm-seq and input are shown below and above the transcript, respectively. Individual paired-end reads within the Nm site window are shown in magnification.



Supplementary Figure 3

Features of the HeLa Nm methylome

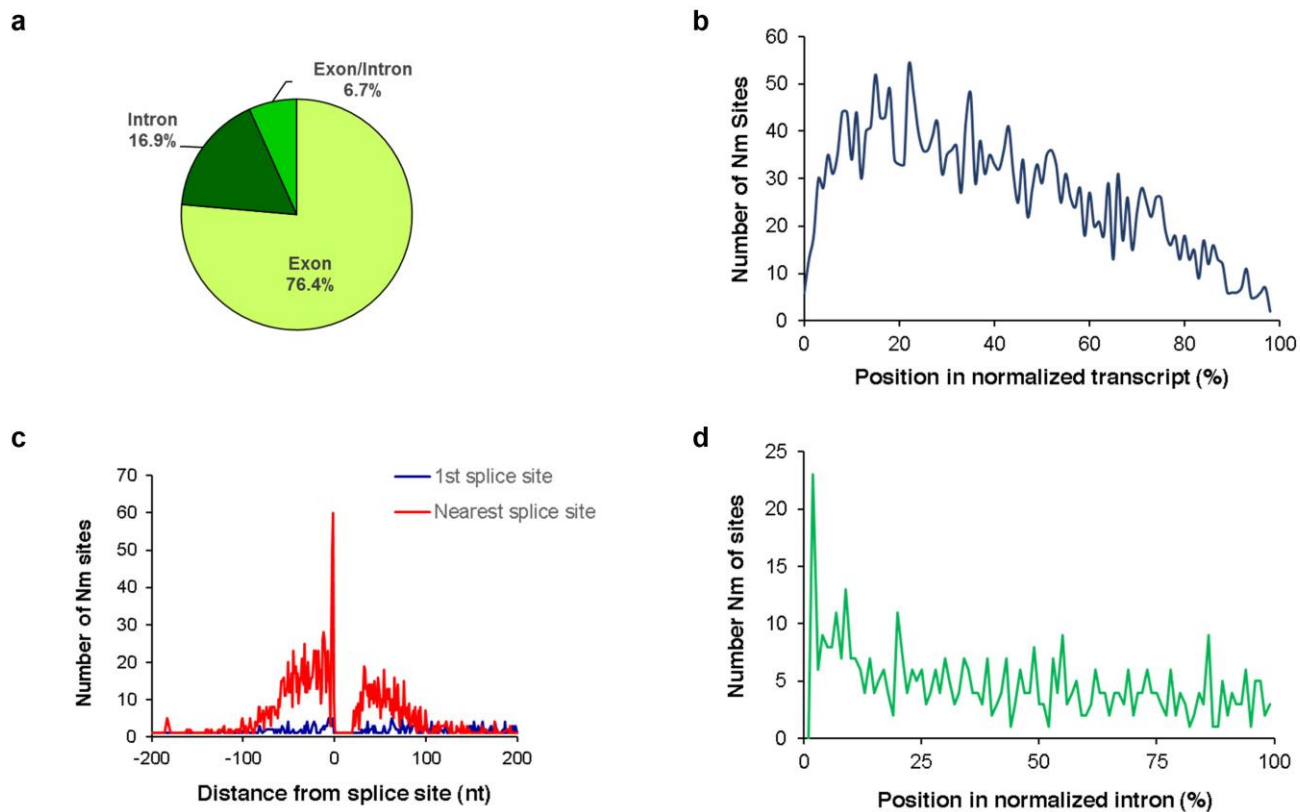
(a) Distribution of 2'-O-methyl sites between the four nucleobases in the various transcript segments and overall. (b) Fraction of Nm sites detected within mRNA and ncRNA. (c) The percentage of methylated genes according to the number of Nm sites per gene. (d) The percentage of methylated genes increases with expression level.



Supplementary Figure 4

RNA secondary structure surrounding Nm sites, m^6Am in mRNA and Gene Ontology (GO) analysis

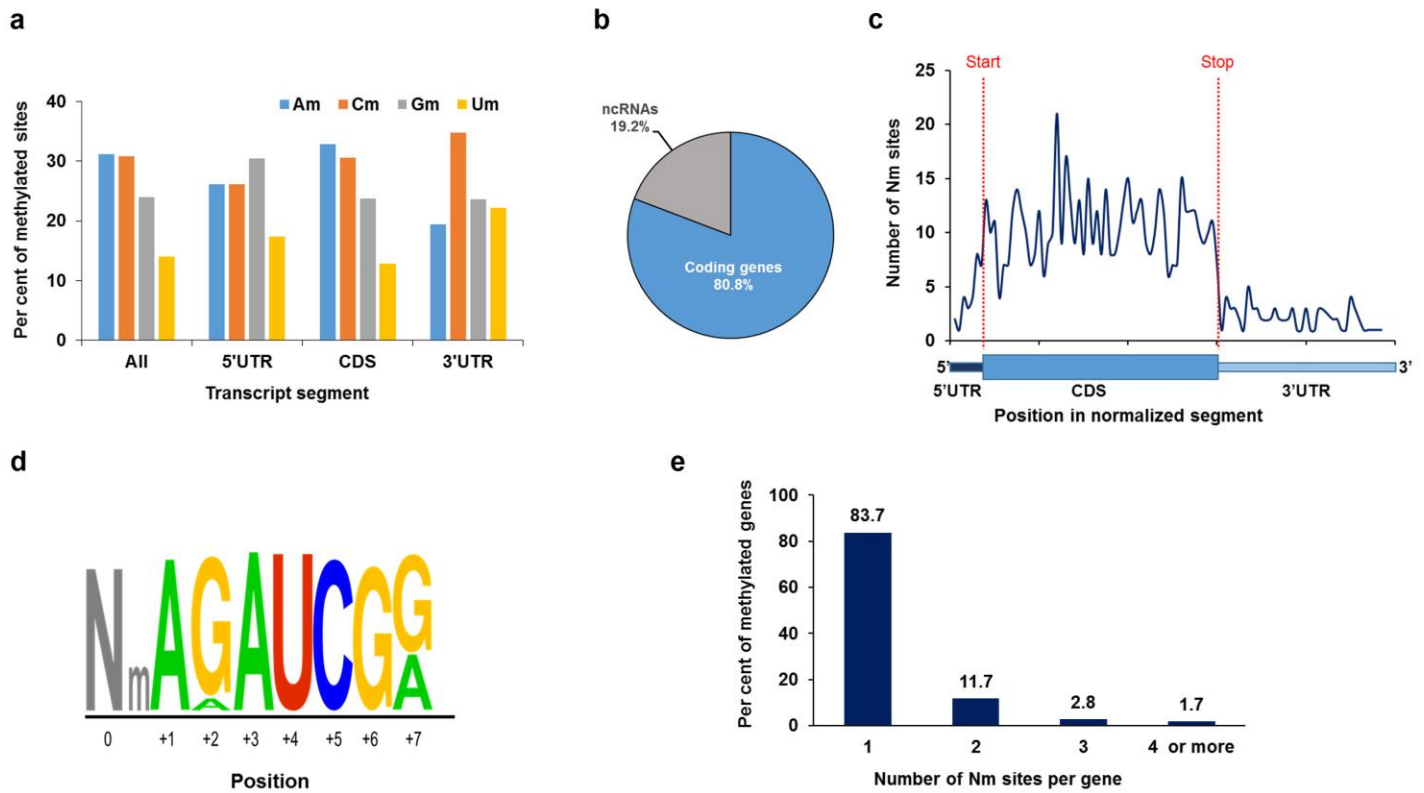
The secondary structures of a 200-nt window centered on Nm sites was analyzed using the Structure Surfer tool based on: **(a)** PARS score **(b)** ds/ssRNA score and **(c)** DMS-seq. **(d)** LC-MS/MS quantification of internal (i.e., excluding the first transcribed nucleotide) m^6A and internal m^6Am in HeLa mRNA. The level of each modified nucleoside is presented as a percentage of the unmodified one. Mean values \pm s.e.m. are shown, $n = 3$. **(e)** GO analysis of Nm-methylated HeLa genes relative to all adequately expressed genes (above the 1st quartile) reveals enrichment of GO terms related to cell-cell interactions, splicing and more (fold enrichment ≥ 2 , Bonferroni corrected $P \leq 0.005$). Fold-enrichment and P values are indicated for each category.



Supplementary Figure 5

Distribution of Nm sites in HeLa mRNA

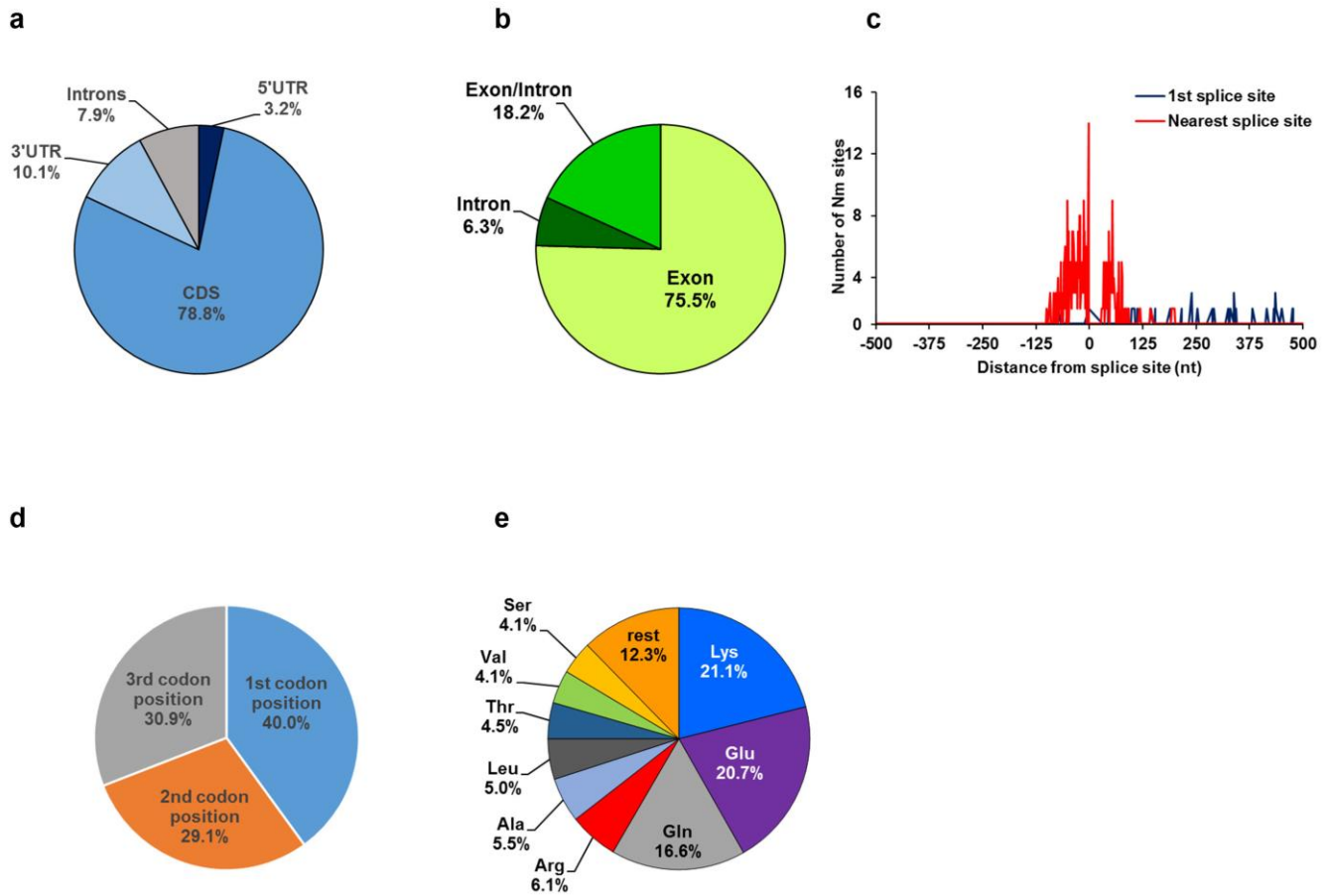
(a) Distribution of Nm sites between exons, introns and alternatively spliced regions. (b) Metagene profile of Nm site distribution along a normalized mRNA transcript. (c) Metagene profile of Nm sites distribution relative to the first and nearest splice sites in a 400-nt non-normalized window. (d) Metagene profile of Nm site distribution along a normalized intron.



Supplementary Figure 6

Features of the Nm methylomes in HEK293 cells (part 1)

(a) Distribution of 2'-O-methyl sites between the four nucleobases in the various transcript segments and overall. (b) Fraction of Nm sites detected within mRNA and ncRNA. (c) Metagenome profile of Nm sites distribution along a normalized mRNA transcript illustrated below. (d) Sequence logo of the most enriched motif identified by HOMER in 58.7% of all HEK293 Nm sites. (e) The percentage of methylated genes according to the number of Nm sites per gene.



Supplementary Figure 7

Features of the Nm methylomes in HEK293 cells (part 2)

(a) HEK293 Nm sites in different transcript segments of coding genes. (b) Distribution of Nm sites between exons, introns and alternatively spliced regions. (c) Metagene profile of Nm sites distribution relative to the first (blue) and nearest (red) splice sites in a 400-nt non-normalized window. (d) Distribution of Nm sites between the three codon positions. (e) Distribution of Nm sites among different amino acid codons.

Amino acid	Codon	# of sites	Sites/position in codon		
			1st	2nd	3rd
Gln	CAG	331	315	6	10
	CAA	51	7	39	5
Glu	GAG	343	327	2	14
	GAA	161	5	145	11
Lys	AAG	402	379	10	13
	AAA	100	3	90	7

Supplementary Table 1

Distribution of HeLa Nm sites in top-modified codons

Amino acid	Codon	# of sites	Sites/position in codon		
			1st	2nd	3rd
Lys	AAG	94	41	4	49
	AAA	24	6	16	2
Glu	GAG	70	31	7	32
	GAA	46	20	25	1
Gln	CAG	84	44	1	39
	CAA	9	1	6	2

Supplementary Table 2

Distribution of HEK293 Nm sites in top-modified codons

Supplementary Note 1

We validated the individual steps of the protocol using 3'-end modified and unmodified model RNA oligonucleotides. Oxidation/elimination resulted in quantitative removal of one nucleoside from 2'-unmodified oligonucleotides leaving a 3'-monophosphate, which was enzymatically removed, again with a quantitative yield (**Fig. 1c**, blue). In contrast, 2'-modified oligonucleotides did not react with the oxidant and were thus resistant to shortening (**Fig. 1c**, red). We further confirmed the differential ligation compatibility of two model oligonucleotides after oxidation/elimination (excluding dephosphorylation): while the 2'-modified oligonucleotide was successfully ligated to the 3' adapter independent of oxidation/elimination, ligation of the 2'-unmodified one was effectively prevented by the prior oxidation/elimination reaction (**Fig. 1d**).

Supplementary Note 2

A comparative assessment of corresponding Receiver Operating Characteristic (ROC) and Matthews Correlation Coefficient (MCC) curves for various coverage thresholds demonstrated high discriminatory power with maximal MCC values 0.86 and 0.73 for the 18S and 28S subunits, respectively (**Supplementary Fig. 1c,d**). These performance parameters are on a par with existing methods¹⁶⁻²⁰ for high-throughput 2'-*O*-methylation mapping in rRNA, and therefore we proceeded to map Nm sites in mRNA.

Supplementary Note 3

Methylated genes constitute a progressively larger fraction of genes as expression increases (**Supplementary Fig. 3d**), in line with the expected parallel increase in detection sensitivity. This feature is different from internal m⁶A, for which transcripts of moderately expressed genes are more likely to be methylated and transcripts of highly expressed genes less likely¹. We failed to observe almost any overlap between Am and m⁶A, which is consistent with exceedingly low level of internal N⁶,2'-*O*-dimethyladenosine (m⁶Am) detected in mRNA from the same cells (**Supplementary Fig. 4d**). Gene ontology analysis identified enrichment of terms related to cell-cell interaction and splicing (**Supplementary Fig. 4e**).

Supplementary Note 4

Two recent CLIP-seq studies found that a sizeable fraction of FBL binding regions are within mRNAs^{20,35}. Overlap of these regions with our dataset of 3,515 high-confidence Nm sites identified 600 and 1,160 Nm sites contained within FBL binding regions ($P = 1.38 \times 10^{-156}$ and $P = 3.77 \times 10^{-175}$, respectively, one sample t-test), raising the possibility that FBL catalyzes methylation of this subset of sites.

Supplementary Note 5

The features of the Nm methylome give rise to several interesting future directions: Nm could be triggered as a response to RNA damage and repair (as in bacteria), it could lead to recoding or affect elongation dynamics based on codon-anticodon interactions in the context of the elongating

ribosome, it could modulate protein binding to single-stranded or double-stranded RNA, regulate diverse processes such as splicing, translation and decay (e.g., no-go decay in case of ribosome stalling). Our discovery adds yet another modification to the known epitranscriptome repertoire and lays the foundations for future functional investigations that parse out the roles of Nm in mRNA.